To be published in Optics Letters:

Title: Tailoring directivity of two-photon spontaneous emission using plasmonic nanoantennas

Authors: Steve SMEETS,Bjorn Maes,Gilles Rosolen

Accepted: 11 February 25

Posted 12 February 25

DOI: https://doi.org/10.1364/OL.539545

Tailoring directivity of two-photon spontaneous emission using plasmonic nanoantennas

STEVE SMEETS[1,*], BJORN MAES[1], AND GILLES ROSOLEN[1]

[1] *Micro- and Nanophotonic Materials Group, Research Institute for Materials Science and Engineering, University of Mons, 20 Place du Parc, Mons B-7000, Belgium*
[*] *Steve.Smeets@umons.ac.be*

Compiled November 18, 2024

We report nanoantenna designs that emit entangled photons of distinct energy from two-photon spontaneous emission (TPSE) in different far-field directions with a high quantum efficiency. To model the designs, we use a framework that computes TPSE spectra of a quantum emitter near arbitrarily shaped nanostructures via the classical computation of the one-photon Purcell factors. A first structure exploits both the dipolar and the quadrupolar mode on a single silver nanorod. A second geometry employs dipolar modes on two perpendicular nanorods. The efficient and directional functionality is useful to develop highly compact, integrated entangled two-photon sources.

http://dx.doi.org/10.1364/ao.XX.XXXXXX

Introduction. Efficient entangled photon sources, especially at telecommunication wavelengths, are essential to test the foundations of quantum mechanics [1] and for many quantum applications [2–5], including computation, teleportation, secure communications, etc. The most common approach to generating entangled photon pairs is the spontaneous parametric down conversion process (SPDC) in nonlinear crystals, in which pump photons are converted into photon pairs of lower energy [5, 6]. However, two-photon spontaneous emission (TPSE), a broadband process that involves the simultaneous emission of two entangled photons from an excited quantum emitter [7], is a promising alternative. Indeed, TPSE sources are theoretically expected to be 3 orders of magnitude more efficient than SPDC sources for equal pump levels [2] because it is a second-order non-resonant process in time-dependent perturbation theory, while SPDC is a third-order non-resonant one. In addition, TPSE can be more flexible for designing sources with given output wavelengths since there is no phase matching condition to satisfy [3]. Furthermore, TPSE is promising for on-chip integrated two-photon sources where one proposes nanostructures coupled to waveguides [8], photonic crystals [9], or cavities [10]. Recently, heralded hyper-entangled (i.e., entanglement in various degrees of freedom verified through a measurement process) photons at telecommunication wavelengths were created using TPSE from Rydberg atoms inside a photonic cavity [3].

Despite that TPSE typically occurs 8 to 10 orders of magnitude slower than the competing spontaneous emission of a single photon [11], it is possible to tailor these processes via the well-known Purcell effect [12] by designing the emitter environment. Thereby, two-photon transitions can outperform single-photon transitions [13] using e.g., plasmonic [11, 14] and phonon polaritonic [15, 16] structures with light confined at the nanoscale. In addition to modifying the TPSE rate, we can tune the system directivity [17, 18] to emit in the far-field, or to couple to a waveguide [8]. For TPSE, nanoantennas provide important degrees of freedom to optimize the emission of different photon energies in separate directions.

In this letter, we propose two designs (see Fig. 1) to emit the two photons from TPSE in specific directions with a quantum efficiency greater than 77 %. First, we combine plasmonic excitations characterized by surface charges exhibiting a dipolar and a quadrupolar aspect in a single silver nanorod, with the emitter positioned at the rod extremity [Fig. 1(a)]. These modes radiate essentially with a dipolar and a quadrupolar radiation pattern, respectively, so the photons are emitted with these different patterns. Second, we exploit the dipolar modes on two perpendicular nanorods with tailored sizes, with the emitter at the corner, to emit in perpendicular directions [Fig. 1(b)]. As proof of concept, we consider the hydrogen atom as the quantum emitter and we study its transition [Fig. 2] from the excited state $4s$ to the final state $2s$. Although our method [19] allows to calculate the electric dipole, magnetic dipole, and electric quadrupole contributions to the TPSE, it is sufficient to calculate the electric dipole one due to the large size of the nanostructures compared to the emitter size [20]. Note that one-photon transitions are forbidden between these states.

Method. To compute the two-photon Purcell effect, i.e., the modification of the two-photon transition rate with respect to the vacuum, we use our previously developed framework [19] which is valid for a quantum emitter at any position and close to arbitrary structures. Thereby, the TPSE rate is given by [19]:

$$\Gamma^{(2)}(\mathbf{R}) = \int_0^{\omega_{eg}} \gamma^{(2)}(\omega;\mathbf{R})\,\mathrm{d}\omega, \tag{1}$$

with ω_{eg} the transition frequency and $\mathbf{R}$ the emitter position (center of its charge distribution). $\gamma^{(2)}(\omega;\mathbf{R})$ is the spectral distribution rate of the emitted quanta that can be written as a

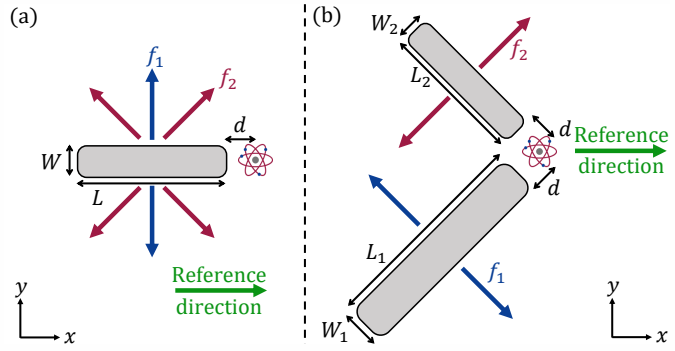

Fig. 1. Quantum emitter near silver nanorods of square cross-section, designed to radiate two photons of frequencies f_1 and $f_2 = 1 - f_1$ with $f_1 \neq f_2$ in different directions. Green arrows denote reference directions for radiation patterns. (a) Emitter positioned on the axis at a distance d from a rod of length L, width W. Dipolar and quadrupolar modes are excited at the frequencies f_1 and f_2, respectively. (b) Emitter on the axes and at a distance d from two perpendicular rods forming an angle of 45° with the x axis. A dipolar mode is excited at f_1 (resp. f_2) on the rod of length L_1 (L_2) and width W_1 (W_2).

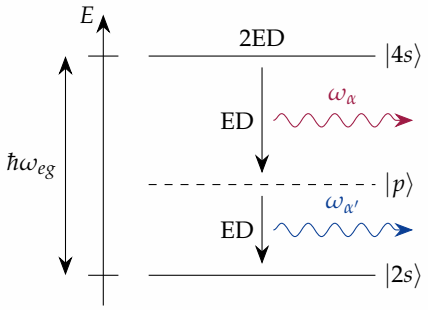

Fig. 2. Energy representation of a two-electric dipole transition (2ED) between the 4s and 2s states of a hydrogen atom. The emitter carries out a first ED transition from its excited state $|4s\rangle$ to a virtual intermediate state, which is of type p due to the selection rules [19], by emitting a photon in the mode α. Then, a second ED transition is carried out to state $|2s\rangle$ of lower energy by emitting a photon in the mode α'. The transition energy is $\hbar\omega_{eg} = 2.55$ eV (wavelength of 486 nm) and the two photons have complementary frequencies: $\omega_\alpha + \omega_{\alpha'} = \omega_{eg}$.

function of the Purcell factors of the two quanta emitted at complementary frequencies [19]:

$$\frac{\gamma^{(2)}(\omega;\mathbf{R})}{\gamma_0^{(2)}(\omega)} = \frac{1}{3}\sum_{i,j=1}^{3} F_{ij}(\omega;\mathbf{R})\, F_{ij}(\omega_{eg}-\omega;\mathbf{R}), \tag{2}$$

where $\gamma_0^{(2)}(\omega)$ is the spectral two-photon decay rate in vacuum. In this expression, the tensor that depends only on the electronic structure of the emitter has been calculated analytically for $s \to s$ transitions [19, 21]. In addition, the tensor F is present for the two quanta emitted at the complementary frequencies ω and $\omega_{eg} - \omega$ and depends only on the photonic environment since it is expressed as a function of Purcell factors [19]:

$$\forall i = j, \quad F_{ii}(\omega;\mathbf{R}) = P_i(\omega;\mathbf{R}), \tag{3}$$

$$\forall i \neq j, \quad F_{ij}(\omega;\mathbf{R}) = P_{ij}(\omega;\mathbf{R}) - \frac{1}{2}\left[P_i(\omega;\mathbf{R}) + P_j(\omega;\mathbf{R})\right], \tag{4}$$

where P_i and P_{ij} denote the Purcell factors related to an electric dipole aligned along the vector $\hat{\mathbf{e}}_i$ and along $\hat{\mathbf{e}}_i + \hat{\mathbf{e}}_j$, where the vectors $\hat{\mathbf{e}}_i$ form an orthonormal basis.

Since the tensor F is symmetric [Eq. (4)], it involves six independent components involving the calculation of the six following Purcell factors: $\{P_x, P_y, P_z, P_{xy}, P_{xz}, P_{yz}\}$ at frequencies comprised between 0 and ω_{eg} (see the limits of integration in Eq. (1)). For the first geometry depicted in Fig. 1(a), due to equivalence between the y and z directions, it is sufficient to calculate the three following components: $\{F_{xx}, F_{yy}, F_{xy}\}$ and so the three following Purcell factors: $\{P_x, P_y, P_{xy}\}$. Furthermore, the Purcell factors can be computed classically by modelling electric dipole point sources in electromagnetic simulations: $P = W/W_0$ with W and W_0 being the powers emitted by the classical source in its environment and in vacuum [12].

Near plasmonic structures, the two-quanta emission is mainly given by three distinct emission pathways: the photon-photon (ph-ph), photon-plasmon (ph-pl), and plasmon-plasmon (pl-pl) channels [22]. These pathways can be calculated via the decomposition of the Purcell factors into radiative and non-radiative parts: $P = P_{\text{rad}} + P_{\text{n-rad}}$ [12, 19]. Furthermore, we define the TPSE quantum efficiency as the ratio between the *two-photon* emission rate (indicating far-field emission) and the total two-quanta emission rate: $\eta^{(2)} := \gamma^{(2)}_{\text{ph-ph}}/\gamma^{(2)}$.

Specifically, we use COMSOL Multiphysics® software based on the finite element method to compute the Purcell factors. The simulation domain is a sphere with a radius equal to twice the transition wavelength λ_t, and perfectly matched layers (PMLs) are defined as an outer layer with a thickness of $\lambda_t/2$. To avoid unphysically sharp edges, the silver nanorods of square cross-section have rounded edges with radius equal to a quarter of their width W. The silver optical response is given by the Drude conductivity $\sigma = \varepsilon_0\tau\omega_p^2/(1 - i\omega\tau)$ with the plasma frequency $\hbar\omega_p = 9.1$ eV and the relaxation rate $\hbar\tau^{-1} = 18$ meV. The classical emitter is positioned at a distance $d = 15$ nm from the extremity of the nanorods and is modelled by a radiating electric point dipole. The Purcell factors are determined through the integration of emitted power on the inner surface of the PMLs for the radiative part and on the surface of a fictional sphere with a 5 nm radius centered on the emitter for the total part (sum of radiative and non-radiative parts). An unstructured tetrahedral mesh is used, where the smallest element has a characteristic size of 1 nm on the structures and on the sphere around the emitter. Calculating the six Purcell factors over 95 frequencies for the system with two nanorods (sizes given below) requires 6×22 GB of RAM and 5 hours using 6×8 cores of an AMD Ryzen Threadripper PRO 5995WX 64-core CPU.

Results and discussion. We design a directional emitter using a single nanorod [Fig. 1(a)] that emits a photon at the frequency f_1 via a dipolar mode of the nanorod, and the second photon at the complementary frequency $f_2 = 1 - f_1$ via a quadrupolar mode of the nanorod, with $f := \omega/\omega_{eg}$ the dimensionless frequency comprised between 0 and 1. We find that this condition is satisfied at $f_1 = 0.34$ ($\lambda = 1.43$ µm) and $f_2 = 0.66$ ($\lambda = 736$ nm) for a 412 nm long and 39 nm wide nanorod. The emission characteristics are presented in Fig. 3.

The strongest Purcell factor is reached with a dipole oriented along x (the nanorod axis), which is plotted in Fig. 3(a). The surface charge density and the 3D radiation pattern (for a dipole along x) at the frequencies f_1 and f_2 of the dipolar and quadrupolar modes are illustrated in Fig. 3(b). In addition to these two

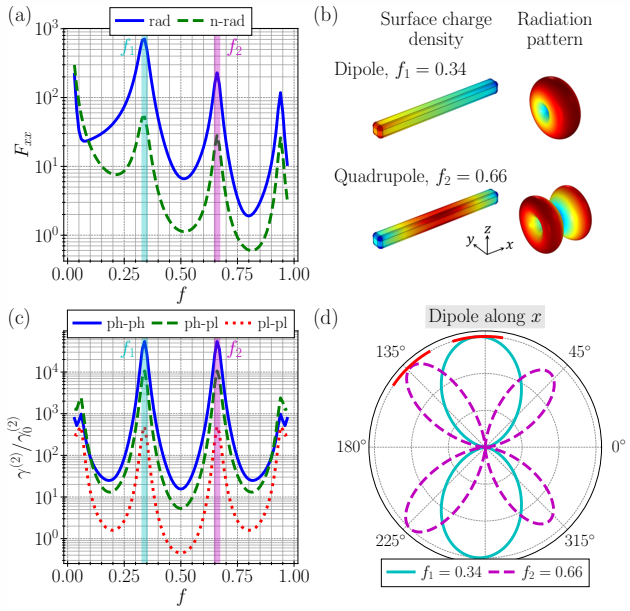

Fig. 3. Single rod results. (a) Radiative (rad) and non-radiative (n-rad) parts of $F_{xx} = P_x$. (b) Surface charge density on the nanorod and radiation pattern for the complementary frequencies f_1 (dipole) and f_2 (quadrupole). (c) Ph-ph, ph-pl, and pl-pl emission channels of the vacuum normalized spectral TPSE rate. The quanta are emitted at the complementary frequencies f and $1-f$, leading to symmetric spectra with respect to $f = 0.5$. (d) Radiation pattern in the XY plane for a dipole along x, identical in the XZ plane, for the complementary frequencies f_1 and f_2 corresponding to the main TPSE peak. The reference direction and the normal vector are the nanorod axis and the z axis, respectively [Fig. 1(a)]. The patterns are calculated using the squared norm of the far-field electric field and are normalized according to their maxima (if a photon is emitted at one frequency, the second one is systematically emitted at the complementary one).

modes, F_{xx} exhibits a sextupolar mode (not shown) at $f = 0.94$.

The vacuum normalized spectral TPSE rate is plotted in Fig. 3(c). Since TPSE involves two quanta emitted at complementary frequencies, the dipolar and quadrupolar modes in Fig. 3(a) both contribute to the main TPSE peaks at the complementary frequencies $f_1 = 0.34$ and $f_2 = 0.66$. At these frequencies, the term involving the component F_{xx} in the TPSE rate calculation [Eq. (2)] dominates, and the others are negligible (contributing less than 0.01 %). Moreover, at the main TPSE peaks, the emission of a pair of photons is enhanced by a factor 5.4×10^4 with respect to the vacuum and the quantum efficiency is $\eta^{(2)} = 83\,\%$. As there is no resonance at the complementary frequency $f = 0.06$ of the sextupolar mode at $f = 0.94$, the emitter is 143 times more likely to decay into two photons emitted at the frequencies f_1 and f_2 than at frequencies $f = 0.06$ and $f = 0.94$. Note also that 65 % of the photons are emitted in the full width at half maximum (FWHM) of the main peaks. The FWHM of a main TPSE peak is equal to $\Delta f = 2.3\,\%$. These values have been calculated by considering the TPSE spectrum which is not normalized with respect to vacuum (not shown).

Since the one-photon Purcell factor P_x is the only non-negligible contribution to the TPSE, the photon pair results mainly from a decay described by two electric dipole transition moments along x [Eq. (2) and Fig. 2]. Indeed, as the initial and final states of the quantum emitter are identical, the selection rules require two transition moments with the same orientation. The most likely is to emit two photons at the frequencies $f_1 = 0.34$ and $f_2 = 0.66$ via a dipolar mode and a quadrupolar mode [Fig. 3(b)], respectively, so the corresponding radiation patterns are drawn in Fig. 3(d). Clearly, the two photons are emitted in different patterns, and thus mainly in distinct directions. Note that positioning the emitter at one extremity of the nanorod results in slightly (left-right) asymmetrical radiation patterns. Quantitatively, we can compute the photon proportion emitted at a given frequency in a cone with an angular width of 25° with axis in the XY plane and forming an angle of ψ with respect to the x axis, corresponding to the maximum of one of the lobes of a radiation pattern. Compared with an isotropic source, 3.0 times more photons are emitted at f_1 within a cone at $\psi = 94°$, while 3.7 times more photons are emitted at f_2 within a cone positioned at 133° (red curves in Fig. 3(d)).

A disadvantage of the single rod is that it is not possible to choose the complementary frequencies of the photons emitted. Indeed, these two frequencies must correspond to the excitation of a dipolar and quadrupolar mode, respectively, which is verified only for one frequency pair. Therefore, we now consider the double-rod design (see Fig. 1(b)), which employs excitation of dipolar modes on two rods of different sizes. This system does not present the restriction mentioned above since we can freely choose the size of the rods to excite the dipolar modes at complementary frequencies, except that overlap with higher-order modes (e.g., quadrupolar modes) must be avoided. Thus, we employ the following parameters: $L_1 = 289$ nm, $W_1 = 36$ nm, $L_2 = 146$ nm, $W_2 = 21$ nm. As a result, there is radiative enhancement via a dipolar mode at the frequency $f_1 = 0.42$ ($\lambda = 1.16$ µm) on the larger rod, and at the complementary frequency $f_2 = 1 - f_1 = 0.58$ ($\lambda = 838$ nm) on the smaller rod, while preventing a frequency overlap between the dipolar mode of the smaller rod with the quadrupolar mode of the larger one.

The strongest Purcell factors are reached with dipoles oriented in the plane of the rods (XY). Thus, the components F_{xx}, F_{yy}, and F_{xy} dominate and are shown in Fig. 4(a-c), while the others (F_{zz}, F_{xz}, and F_{yz}) are negligible. The peaks at $f_1 = 0.42$ and $f = 0.84$ correspond to a dipolar and a quadrupolar mode on the larger rod, while the peak at $f_2 = 0.58$ is a dipolar mode on the smaller rod. Note that $F_{yy}(f_1) > F_{xx}(f_1)$ and that $F_{xx}(f_2) > F_{yy}(f_2)$ because the charge surface density on the two-rod system are asymmetric and symmetric, respectively. The vacuum normalized spectral TPSE rate is shown in Fig. 4(d). The dipolar peaks in Fig. 4(a-c) both contribute to the TPSE peaks at the complementary frequencies f_1 and f_2. At these frequencies, the terms involving the components F_{xx}, F_{yy}, and F_{xy} in the TPSE rate calculation [Eq. (2)] dominate, and the others are negligible (contributing less than 0.01 %). Moreover, at the main TPSE peaks, the emission of a pair of photons is enhanced by a factor 7.5×10^4 with respect to vacuum, and the quantum efficiency is large: $\eta^{(2)} = 77\,\%$. In addition, the emitter is 120 times more likely to decay into two photons emitted at the frequencies f_1 and f_2 than at the frequency $f = 0.84$ of the quadrupolar mode. Note also that 61 % of the photons are emitted in the full width at half maximum (FWHM) of the main peaks. The FWHM of a main TPSE peak is equal to $\Delta f = 2.4\,\%$.

Since there is no enhancement with dipoles oriented perpendicular to the XY plane comprising the system [Fig. 1(b)], the photon pair results mainly from a decay described by two electric dipole transition moments in the XY plane [Fig. 2]. Moreover, the most likely is to emit two photons at the frequencies

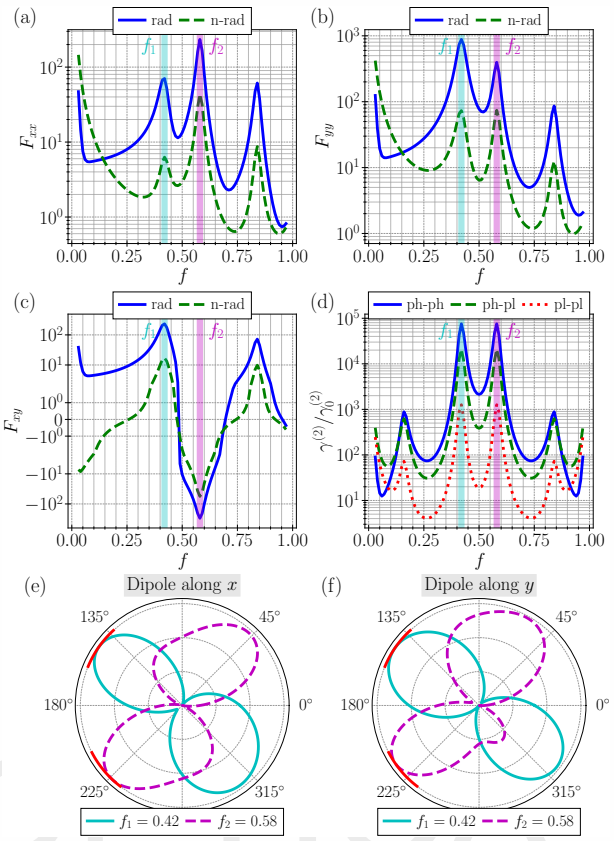

Fig. 4. Double rod results. Radiative (rad) and non-radiative (n-rad) parts of (a) $F_{xx} = P_x$, (b) $F_{yy} = P_y$, and (c) $F_{xy} = P_{xy} - (P_x + P_y)/2$. (d) Ph-ph, ph-pl, and pl-pl emission channels of the vacuum normalized spectral TPSE rate (symmetric around 0.5). (e, f) Radiation pattern in the XY plane for a dipole along x and y for the complementary frequencies f_1 and f_2 corresponding to the main TPSE peak. The reference direction and the normal vector are the x and z axis, respectively [Fig. 1(b)].

$f_1 = 0.42$ and $f_2 = 0.58$ via the dipolar mode on each rod. The corresponding radiation patterns are drawn in Fig. 4(e,f) for electric dipole transition moments oriented along x and y. Thereby, whatever the orientation (in the XY plane) of the transition moments, the two photons are emitted with asymmetric dipolar radiation patterns rotated about 90 degrees to each other, thus in perpendicular directions. The asymmetry arises because at both frequencies the surface charge density is non-zero on the rods, even though they are not designed to have a dipole mode at the other frequency. Using the same methodology as for the one-rod system for the comparison with an isotropic source, for a transition moment along x (resp. y), 2.9 (3.0) times more photons are emitted at f_1 within a cone at $\psi = 145°$, while 2.3 (2.4) times more photons are emitted at f_2 within a cone positioned at 220° (red curves in Fig. 4(e,f)).

Conclusion. TPSE is a promising alternative to conventional SPDC to create efficient and flexible entangled photon sources. An important challenge for TPSE sources is for systems to exhibit directivity in different directions at different frequencies. Here, we propose two subwavelength silver nanorod designs in order to emit the TPSE photons in distinct directions. The single-rod mechanism exploits a dipolar and quadrupolar mode, while the double-rod employs dipolar modes on perpendicular rods of different size. The double-rod design offers greater freedom in choosing the frequencies. Both structures feature a high quantum efficiency ($> 77\,\%$) with an enhancement of more than four orders of magnitude of the TPSE rate. For application, one can optimize the radiation patterns to place waveguides, detectors, etc. in the maximum emission directions. These systems use the directivity of dipoles and quadrupoles, which is weaker than what is reachable with e.g., Yagi-Uda [23] nanoantennas and hybrid metal-dielectric nanostructures [18]. Thus, the directivity may be improved by more complex geometries, e.g., considering an extra dielectric structure [24]. Moreover, the system should also be optimized for the degree of energy entanglement, which in the antenna systems depends on the observation angle. The precise relation between directionality and entanglement is an interesting subject for future work, as hyper-entanglement with polarization degrees e.g., could be possible. Finally, we considered a hydrogen-like emitter as a proof of concept, but the findings can be applied to other quantum emitters.

Funding. Fonds De La Recherche Scientifique - FNRS (Research project T.0166.20); Action de Recherche Concertée (Project ARC-21/25 UMONS2).

Disclosures. The authors declare no conflicts of interest.

Data availability. Data underlying the results may be obtained from the authors upon reasonable request.

REFERENCES

1. P. Shadbolt, J. C. F. Mathews, A. Laing, and J. L. O'Brien, Nat. Phys. **10**, 278 (2014).
2. A. Hayat, P. Ginzburg, and M. Orenstein, Phys. Rev. B **76**, 035339 (2007).
3. S. Ghosh, N. Rivera, G. Eisenstein, and I. Kaminer, Light. Sci. & Appl. **10**, 100 (2021).
4. Y. Wang, S. Pandey, C. H. Greene, and N. Shivaram, Phys. Rev. Res. **4**, L032038 (2022).
5. C. Couteau, Contemp. Phys. **59**, 291 (2018).
6. P. G. Kwiat, K. Mattle, H. Weinfurter, *et al.*, Phys. Rev. Lett. **75**, 4337 (1995).
7. M. Göppert-Mayer, Ann. der Physik **401**, 273 (1931).
8. G. P. Agrawal, *Nonlinear fiber optics*, Quantum electronics–principles and applications (Elsevier / Academic Press, Amsterdam ; Boston, 2007), 4th ed.
9. Y. Zeng, Y. Fu, X. Chen, *et al.*, J. Opt. Soc. Am. B **24**, 1365 (2007).
10. A. Dousse, J. Suffczyński, A. Beveratos, *et al.*, Nature **466**, 217 (2010).
11. N. Rivera, I. Kaminer, B. Zhen, *et al.*, Science **353**, 263 (2016).
12. L. Novotny and B. Hecht, *Principles of Nano-Optics* (Cambridge University Press, Cambridge, 2012), 2nd ed.
13. N. Rivera and I. Kaminer, Nat. Rev. Phys. **2**, 538 (2020).
14. A. N. Poddubny, P. Ginzburg, P. A. Belov, *et al.*, Phys. Rev. A **86**, 033826 (2012).
15. N. Rivera, G. Rosolen, J. D. Joannopoulos, *et al.*, Proc. National Acad. Sci. **114**, 13607 (2017).
16. N. Rivera, T. Christensen, and P. Narang, Nano Lett. **19**, 2653 (2019).
17. A. F. Koenderink, ACS Photonics **4**, 710 (2017).
18. A. Barreda, F. Vitale, A. E. Minovich, *et al.*, Adv. Photonics Res. **3**, 2100286 (2022).
19. S. Smeets, B. Maes, and G. Rosolen, Phys. Rev. A **107**, 063516 (2023).
20. Y. Zhang, Z.-C. Dong, and J. Aizpurua, The J. Phys. Chem. C **124**, 4674 (2020).
21. Y. Muniz, F. S. S. da Rosa, C. Farina, *et al.*, Phys. Rev. A **100**, 023818 (2019).
22. Y. Muniz, A. Manjavacas, C. Farina, *et al.*, Phys. Rev. Lett. **125**, 033601 (2020).
23. A. F. Koenderink, Nano Lett. **9**, 4228 (2009).
24. E. Rusak, I. Staude, M. Decker, *et al.*, Appl. Phys. Lett. **105**, 221109 (2014).

FULL REFERENCES

1. P. Shadbolt, J. C. F. Mathews, A. Laing, and J. L. O'Brien, "Testing foundations of quantum mechanics with photons," Nat. Phys. **10**, 278–286 (2014).
2. A. Hayat, P. Ginzburg, and M. Orenstein, "High-rate entanglement source via two-photon emission from semiconductor quantum wells," Phys. Rev. B **76**, 035339 (2007).
3. S. Ghosh, N. Rivera, G. Eisenstein, and I. Kaminer, "Creating heralded hyper-entangled photons using Rydberg atoms," Light. Sci. & Appl. **10**, 100 (2021).
4. Y. Wang, S. Pandey, C. H. Greene, and N. Shivaram, "Attosecond entangled photons from two-photon decay of metastable atoms: A source for attosecond experiments and beyond," Phys. Rev. Res. **4**, L032038 (2022).
5. C. Couteau, "Spontaneous parametric down-conversion," Contemp. Phys. **59**, 291–304 (2018).
6. P. G. Kwiat, K. Mattle, H. Weinfurter, *et al.*, "New High-Intensity Source of Polarization-Entangled Photon Pairs," Phys. Rev. Lett. **75**, 4337–4341 (1995).
7. M. Göppert-Mayer, "Über Elementarakte mit zwei Quantensprüngen," Ann. der Physik **401**, 273–294 (1931).
8. G. P. Agrawal, *Nonlinear fiber optics*, Quantum electronics–principles and applications (Elsevier / Academic Press, Amsterdam ; Boston, 2007), 4th ed.
9. Y. Zeng, Y. Fu, X. Chen, *et al.*, "Highly efficient generation of entangled photon pair by spontaneous parametric downconversion in defective photonic crystals," J. Opt. Soc. Am. B **24**, 1365 (2007).
10. A. Dousse, J. Suffczyński, A. Beveratos, *et al.*, "Ultrabright source of entangled photon pairs," Nature **466**, 217–220 (2010).
11. N. Rivera, I. Kaminer, B. Zhen, *et al.*, "Shrinking light to allow forbidden transitions on the atomic scale," Science **353**, 263–269 (2016).
12. L. Novotny and B. Hecht, *Principles of Nano-Optics* (Cambridge University Press, Cambridge, 2012), 2nd ed.
13. N. Rivera and I. Kaminer, "Light-matter interactions with photonic quasiparticles," Nat. Rev. Phys. **2**, 538–561 (2020).
14. A. N. Poddubny, P. Ginzburg, P. A. Belov, *et al.*, "Tailoring and enhancing spontaneous two-photon emission using resonant plasmonic nanostructures," Phys. Rev. A **86**, 033826 (2012).
15. N. Rivera, G. Rosolen, J. D. Joannopoulos, *et al.*, "Making two-photon processes dominate one-photon processes using mid-IR phonon polaritons," Proc. National Acad. Sci. **114**, 13607–13612 (2017).
16. N. Rivera, T. Christensen, and P. Narang, "Phonon Polaritonics in Two-Dimensional Materials," Nano Lett. **19**, 2653–2660 (2019).
17. A. F. Koenderink, "Single-Photon Nanoantennas," ACS Photonics **4**, 710–722 (2017).
18. A. Barreda, F. Vitale, A. E. Minovich, *et al.*, "Applications of Hybrid Metal-Dielectric Nanostructures: State of the Art," Adv. Photonics Res. **3**, 2100286 (2022).
19. S. Smeets, B. Maes, and G. Rosolen, "General framework for two-photon spontaneous emission near plasmonic nanostructures," Phys. Rev. A **107**, 063516 (2023).
20. Y. Zhang, Z.-C. Dong, and J. Aizpurua, "Influence of the Chemical Structure on Molecular Light Emission in Strongly Localized Plasmonic Fields," The J. Phys. Chem. C **124**, 4674–4683 (2020).
21. Y. Muniz, F. S. S. da Rosa, C. Farina, *et al.*, "Quantum two-photon emission in a photonic cavity," Phys. Rev. A **100**, 023818 (2019).
22. Y. Muniz, A. Manjavacas, C. Farina, *et al.*, "Two-Photon Spontaneous Emission in Atomically Thin Plasmonic Nanostructures," Phys. Rev. Lett. **125**, 033601 (2020).
23. A. F. Koenderink, "Plasmon Nanoparticle Array Waveguides for Single Photon and Single Plasmon Sources," Nano Lett. **9**, 4228–4233 (2009).
24. E. Rusak, I. Staude, M. Decker, *et al.*, "Hybrid nanoantennas for directional emission enhancement," Appl. Phys. Lett. **105**, 221109 (2014).